ACS APPLIED MATERIALS & INTERFACES

Research Article

www.acsami.org

Impact of Sn(S,Se) Secondary Phases in $Cu_2ZnSn(S,Se)_4$ Solar Cells: a Chemical Route for Their Selective Removal and Absorber Surface Passivation

Haibing Xie,[†] Yudania Sánchez,[†] Simón López-Marino,[†] Moisés Espíndola-Rodríguez,[†] Markus Neuschitzer,[†] Diouldé Sylla,[†] Andrew Fairbrother,[†] Victor Izquierdo-Roca,[†] Alejandro Pérez-Rodríguez,[†,‡] and Edgardo Saucedo*,[†]

[†]IREC, Catalonia Institute for Energy Research, Jardins de les Dones de Negre 1, 2a, 08930 Sant Adrià del Besòs, Spain

[‡]IN2UB, Departament d'Electrònica, Universitat de Barcelona, Martí i Franquès 1-11, 08028 Barcelona, Spain

Supporting Information

ABSTRACT: The control and removal of secondary phases is one of the major challenges for the development of $Cu_2ZnSn(S,Se)_4$ (CZTSSe)-based solar cells. Although etching processes have been developed for Cu(S,Se), Zn(S,Se), and CuSn(S,Se) secondary phases, so far very little attention has been given to the role of Sn(S,Se). In this paper, we report a chemical route using a yellow $(NH_4)_2S$ solution to effectively remove Sn(S,Se). We found that Sn(S,Se) can form on the surface either because of stoichiometric deviation or by condensation. After etching, the efficiency of devices typically increases between 20 and 65% relative to the before etch efficiencies. We achieved a maximum 5.9% efficiency in Se-rich CZTSSe-based devices. It is confirmed that this feature is related not only to the removal of Sn(S,Se) but also to the unexpected passivation of the surface. We propose a phenomenological model for this passivation, which may open new perspectives for the development of CZTSSe-based solar cells.

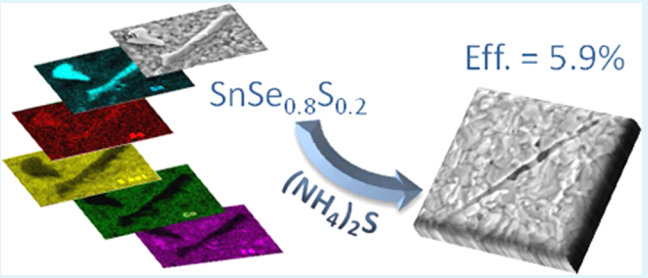

KEYWORDS: *thin films, solar cells, kesterites, $Cu_2ZnSn(S,Se)_4$, secondary phases, Sn(S,Se), chemical etching*

INTRODUCTION

As an ideal candidate for substituting $CuIn_{1-x}Ga_x(S,Se)_2$ (CIGSSe) solar cells due to its earth-abundant and low-toxic constituent elements, $Cu_2ZnSn(S,Se)_4$ (CZTSSe) solar cells are developing very quickly, recently achieving a record efficiency that exceeds 12%.[1] The technological applications of this family of materials range from solar cells to counter electrodes for dye-sensitized solar cells, photoelectrochemical hydrogen production, etc.,[2−4] because of its capability of covering a wide range of band gaps depending on the ratio of S/Se. However, this fascinating as well as complex material exhibits intrinsic properties that complicate its future development. Among these properties, it is important to mention the extremely narrow single-phase existence zone in the phase diagram, the off-stoichiometry conditions used for the preparation of high-efficiency devices (Zn-rich and Cu-poor composition), and the nonequilibrium conditions used during thermal treatments.[5−7] Because of these peculiarities, secondary phases like ternary CuSn(S,Se) and binary Zn(S,Se), Cu(S,Se), and Sn(S,Se) are prone to appearing in the as-prepared absorbers and have already been detected in several works.[1,7−10] If present, these secondary phases can potentially degrade the performance of solar cells, as has been recently observed.[10−12] They may be present either at the interfaces (surface and back contact) or in the bulk, and in fact there are several reports confirming their possible presence along the whole thickness of the films (see, for example, refs 11 and 12 for S and Se compounds, respectively).

When present in the back region or in the bulk,[11] the detrimental effects of secondary phases cannot be avoided, and in fact prevention is probably the only solution, by choosing idealized synthesis conditions: precursors, composition, process parameters, post-treatments, etc. Conversely, when present on the surface, one of the solutions is to remove them by etching. KCN etching is now a daily routine for CIGSSe processing, which can effectively remove Cu(S,Se) also for kesterites.[13−15] Br_2/MeOH was reported to remove Cu−Sn−Se-related secondary phases.[16,17] For ZnS, a 5−10% (75 °C) hot HCl solution is a useful way of selectively removing it.[18] For ZnSe removal, an oxidation route using $KMnO_4/H_2SO_4$ followed by a Na_2S solution rinse was developed, and its effectiveness was shown.[19] Table 1 shows the summary of the most interesting etching routes developed up to now for CIGSSe and CZTSSe solar cells.

Received: May 5, 2014
Accepted: July 17, 2014
Published: July 17, 2014

Table 1. Summary of the Etching Procedures for CIGSSe and CZTSSe Solar Cells

secondary phases	band gap (eV)	potential detriment	etching routes	etching reactions	ref
$Cu_x(S,Se)$ $(1 \le x \le 2)$	1.2–2.2	shunted devices	5–10% (w/v) KCN, RT, 0.5–30 min	$2CuS(Se)(s) + 5KCN(aq) + 2KOH(aq) = 2KCu(CN)_2(aq) + 2K_2S(Se)(aq) + KCNO(aq) + H_2O(l)$	13–15
ZnS	3.7	decrease J_{sc}, increase R_s	5–10% (v/v) HCl, 75 °C, 5–10 min	$2HCl(aq) + ZnS(s) = ZnCl_2(aq) + H_2S(g)$	18
ZnSe	2.7	decrease J_{sc}, increase R_s	$KMnO_4$(0.01 M)/H_2SO_4 (1 M), 30–40 s, and then Na_2S (1 M), 1 min, RT	$8H_2SO_4(aq) + 2KMnO_4(aq) + 5ZnSe(s) = 5Se(s) + 5ZnSO_4(aq) + 2MnSO_4(aq) + K_2SO_4(aq) + 8H_2O(l)$ and $6NaOH(aq) + 3Se(s) = Na_2SeO_3(aq) + 2Na_2Se(aq) + 3H_2O(l)$	19
Cu–Sn–Se (Cu_2SnSe_3, Cu_3SnSe_4)	0.8–1.0	reduce V_{oc}	0.02 M Br_2/MeOH, RT		16 and 17

However, the development of a method for the removal of Sn(S,Se) secondary phases is still a pending task presumably because this secondary phase occurs to a lesser extent than Cu(S,Se) in CIGSSe and Zn(S,Se) in CZTSSe absorbers. Nevertheless, its presence has been noticed in other literature cases.[20,21]

Sn(S,Se) is a low-band-gap phase with E_g approximately equal to 1 eV (this value was reported for a 1:1 stoichiometry compound; other stoichiometries typically exhibit band gaps between 1.1 and 2.5 eV).[22] If this phase is located in the CZTSSe/CdS interface, some subenergy levels will form and thus V_{oc} of the devices will be pulled down, although, in fact, the impact of Sn(S,Se) on the solar cell properties has not been thoroughly investigated yet. In addition, because it is common now to use Sn or Sn(S,Se) to suppress Sn loss during thermal treatment,[23] it is possible that an excess of Sn(S,Se) in the atmosphere may condense onto the surface of as-prepared absorbers during the cooling process. Then the occurrence of this secondary phase may happen by both composition- and/or process-related issues.

During the synthesis of CZTSSe absorbers with the methodology used in this paper and published elsewhere,[24] it was found that there are no Zn(S,Se) phases on the surface of Se-rich CZTSSe films, while Sn(S,Se) may be detected. In consideration of this problem, in this paper a chemical route to selectively remove Sn(S,Se) with a $(NH_4)_2S$ etching solution is presented, and optoelectronic properties before and after etching are discussed. We will demonstrate that the etching is highly effective at removing Sn(S,Se) secondary phases and also, as an additional novel feature, the solution is very useful in effectively passivating the CZTSSe surface.

EXPERIMENTAL SECTION

Metallic Precursor Preparation. Cu/Sn/Cu/Zn precursor stacks were deposited by direct-current (dc) magnetron sputtering (Ac450 Alliance Concepts) onto Mo-coated soda-lime glass (10 × 10 cm^2; 800 nm thickness; $R\square$ = 0.25 Ω/□). The conditions for the deposition of each metal can be found elsewhere.[18,19] Moreover, before metallic precursor deposition, the i-ZnO (10 nm) layer was deposited onto the Mo surface to minimize detrimental reactions between Mo and CZTSSe absorbers during high-temperature annealing.[12] Determined by X-ray fluorescence (XRF; Fisherscope XVD), the metallic stacks were approximately 600 nm thick, with composition ratios of Cu/(Zn + Sn) ≈ 0.8 and Zn/Sn ≈ 1.2.

Absorber Preparation. For solid solution CZTSSe absorbers, metallic precursors were reactively annealed in a graphite box at 550 °C, 1 mbar argon atmosphere for 30 min, and using two crucibles, one with a mixture of selenium (48 mg, Alfa-Aesar, 99.999%) and sulfur powder (2 mg, Alfa-Aesar, 99.995%) and the other with tin powder (5 mg, Alfa-Aesar, 99.999%). The ratio of S/(S + Se) in solid solution CZTSSe absorbers used in this paper was 0.45–0.55, as estimated by X-ray diffraction (XRD), which corresponds to a band gap of 1.22–1.27 eV. Varying the cooling down step of the annealing process, we have produced two types of samples: with low (CZTSSe1) and high (CZTSSe2) quantities of Sn(S,Se) on the surface. Using a natural cooling down step under relatively high vacuum (1×10^{-3} bar), we produced CZTSSe1 samples with little Sn(S,Se) on the surface, whereas using a fast cooling down process under ambient pressure, we obtained CZTSSe2-type samples, with a high quantity of the Sn(S,Se) secondary phase on the surface.

Etching Treatments. Etching of the absorbers was performed at room temperature using a $(NH_4)_2S$ [4–22% (w/w), Alfa-Aesar] aqueous solution or KCN [2% (w/v)] or Na_2S (1 M) solutions for 1 min in all cases. The solutions were stirred during the whole etching process.

Solar Cell Fabrication. Solar cells were assembled by depositing CdS (50−60 nm) by chemical bath deposition onto CZTSSe absorbers, followed by the pulsed dc magnetron sputtering deposition of intrinsic ZnO (50 nm) and ZnO:Al (450 nm, 25 Ω/□; CT100 Alliance Concepts).

Characterization. Inspection of the surface using Raman spectroscopy with three excitation wavelengths (532, 458, and 325 nm) allows us to confirm the absence of Cu(S,Se) and Zn(S,Se) secondary phases on the surface of both types of samples. In all cases, a Horiba Jobin−Yvon T64000 spectrometer at a backscattering configuration was used, and the excitation power density was kept below 100 kW/cm^2 to minimize the presence of thermal effects in the spectra. The scanning electron microscopy (SEM) images were obtained through a Zeiss series Auriga microscope using an accelerating voltage of 10 kV. Energy-dispersive X-ray spectroscopy (EDS; Oxford Instruments, X-Max) was performed using 10 and 20 kV in the working distance 5−8 mm. XRD measurements were performed using a Siemens D500 diffractometer in a 2θ configuration ranging from 10° to 80°. For the optoelectronic characterization, cells (3 × 3 mm^2) were scribed, and the illuminated $I-V$ curves were obtained using an ABET Technologies Sun 3000 Class AAA solar simulator. The external quantum efficiency (EQE) of the devices was performed on a Bentham PVE300 system without a bias voltage or with a bias voltage of −1 V.

RESULTS AND DISCUSSION

Secondary Phases on the Surface of CZTSSe Absorbers. Parts a and b of Figure 1 show the SEM images and EDS mappings of two different types of features observed on the surface of the typical as-annealed CZTSSe films, including the quantification of Cu, Zn, Sn, S, and Se. In particular, Figure 1a shows the typical phase with a rodlike shape, integrated into the surface of the CZTSSe film (type 1), whereas Figure 1b shows the typical phase with approximately round or semicircular shape, which probably originates from Sn(S,Se) condensation from the annealing atmosphere (type 2), as we will show later. EDS mappings performed in the surrounding area that includes these morphologies clearly demonstrate that these two kinds of phases are formed by Sn, Se, and S, suggesting that they are Sn(S,Se) and/or Sn−Se and Sn−S mixed secondary phases. Quantification with EDS shows that the atomic ratio is approximately Sn:Se:S ≈ 50:40:10 in both cases [see also the Supporting Information (SI), part 1], suggesting that these two phases are probably $SnSe_{0.8}S_{0.2}$. This agrees with the phase diagram of both systems (Sn−S and Sn−Se), where under the conditions used in this work, SnS and SnSe are the stable phases.[25,26] The same analysis performed at several points on the CZTSSe layer (excluding these features) allows us to quantify the average kesterite composition: Cu/(Zn + Sn) = 1.03, Zn/Sn = 1.02, and S/(S + Se) = 0.58 (the last ratio is in good agreement with the values obtained by XRD). It is important to remark that both types of Sn(S,Se) features are present in all absorbers used in this paper and that the composition of these absorbers is approximately the same. As we will show in the next section, the removal of both types of Sn(S,Se) features from the CZTSSe surface leads to different consequences on the etched surface.

Figure 2 shows the XRD and Raman spectra of typical as-annealed CZTSSe absorbers. The XRD pattern (Figure 2a) shows that the as-annealed films contain Sn(S,Se) as the secondary phase. In fact, the peak labeled as 3 in the figure presents a slight shift toward high angles with respect to the (400) diffraction peak of SnSe (PDF 00-048-1224), confirming

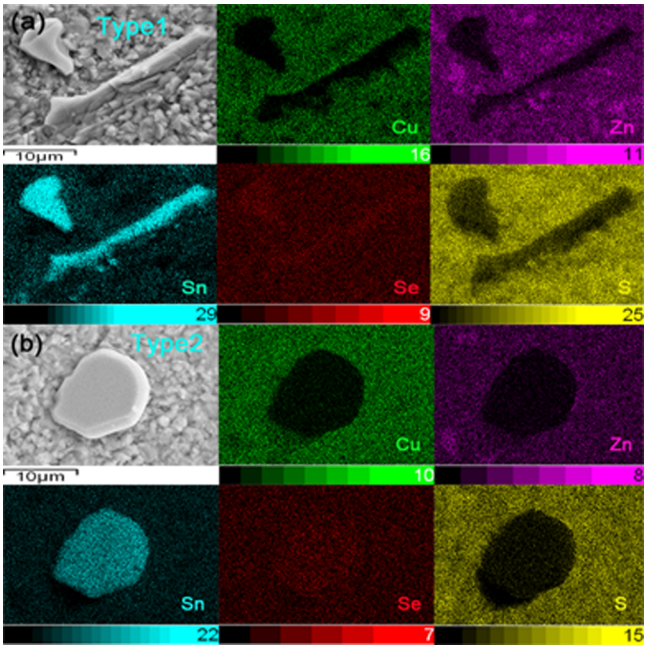

Figure 1. SEM images and EDS mappings of features with different morphologies observed on the surface of CZTSSe absorbers: (a) type 1, encrusted Sn(S,Se); (b) type 2, overgrowth originating from the condensation of Sn(S,Se) from the annealing atmosphere. Different color codes for the intensity of each element are included (Cu in green, Zn in violet, Sn in light blue, Se in red, and S in yellow), from black (no presence of the element) to full color scale (presence of the element).

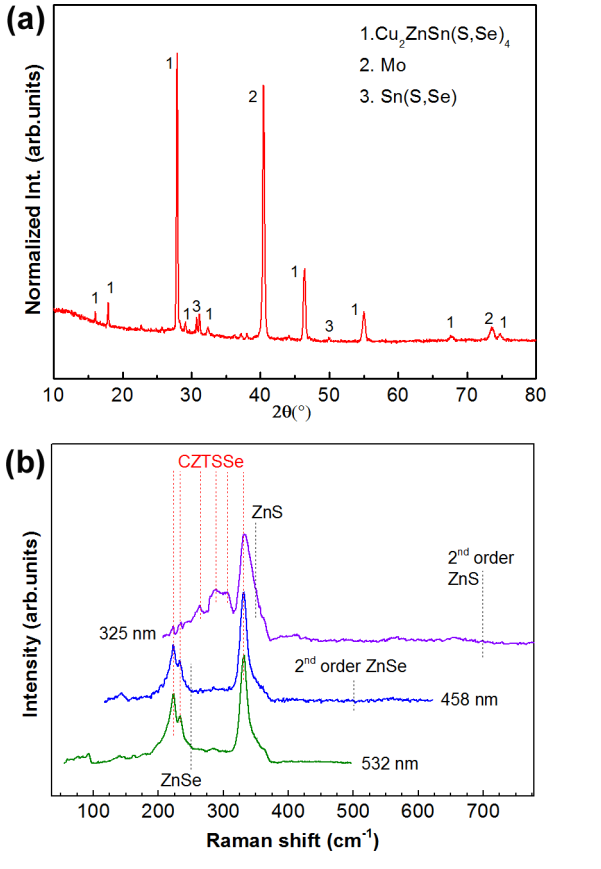

Figure 2. (a) XRD pattern of typical CZTSSe absorbers. (b) Raman spectra of typical CZTSSe absorbers with 532, 458, and 325 nm excitation light.

dx.doi.org/10.1021/am502609c | ACS Appl. Mater. Interfaces 2014, 6, 12744−12751

the presence of some S in this secondary phase. Additionally, this is in agreement with the SEM and EDS results that show the formation of Se-rich Sn(S,Se) together with the main kesterite phase. To unambiguously demonstrate the absence of secondary phases other than Sn(S,Se) on the surface, Raman spectra (Figure 2b) were obtained using three different wavelengths: 532, 458, and 325 nm. Raman with 532 nm is useful for detecting kesterites and Cu(S,Se) secondary phases, while 458 and 325 nm are highly sensitive to detection of ZnSe and ZnS, respectively.[27−30] As is shown in the literature, even tiny ZnSe or ZnS quantities on the surface can be detected using these resonant Raman conditions (peaks at 249 and 500 cm^{-1} correspond to ZnSe, and those at 348 and 697 cm^{-1} correspond to ZnS).[31] From Figure 2b, we can conclude that the CZTSSe surface of the samples under study in this work is free of Cu_xS, Cu_xSe ($x < 1.8$), ZnSe, and ZnS. In particular, the absence of the characteristic 260 cm^{-1} peak in the spectrum acquired using a 532 nm excitation wavelength confirms that a Cu_xSe secondary phase is not present on the surface (green spectrum in Figure 2b).[27] Additionally, the absence of the first-order (249 cm^{-1}) and second-order (500 cm^{-1}) peaks of ZnSe using a 458 nm excitation wavelength (blue spectrum in Figure 2b), as well as the first-order (348 cm^{-1}) and second-order (697 cm^{-1}) peaks of ZnS using a 325 nm excitation wavelength (violet spectrum in Figure 2b), allows us to discard the presence of these two secondary phases on the CZTSSe surface. The presence of ternary CuSn(S,Se) phases cannot be discarded, but considering the imposed Zn-rich and Cu-poor compositional conditions, their formation is highly unexpected. Thus, in these types of samples, Sn binaries are the only secondary phase on the surface, namely, Sn(S,Se), being ideal for the study of the etching process and the influence of Sn(S,Se) on CZTSSe solar cell parameters. This phase has already been observed in the literature by other authors, indicating that its formation can occur during different standard processes (see, for example, refs 20 and 21).

Removal of Sn(S,Se) Secondary Phases. To demonstrate the effectiveness of the $(NH_4)_2S$ etching, as-annealed layers were submitted to processes with different etchant solutions. Figure 3 shows the XRD diffractogram of CZTSSe absorbers before and after etching with different solutions [KCN, Na_2S, and $(NH_4)_2S$], as described in the Experimental Section. From Figure 3, it is clear that KCN and Na_2S etchings are not effective at removing Sn(S,Se), while after etching in a 22% (w/w) $(NH_4)_2S$ solution for 1 min, Sn(S,Se) is removed from the surface. The results show that the peak intensities of CZTSSe barely change before and after $(NH_4)_2S$ etching, which indicates the selective removal of Sn(S,Se), suggesting that the main kesterite phase is slightly or even not affected.

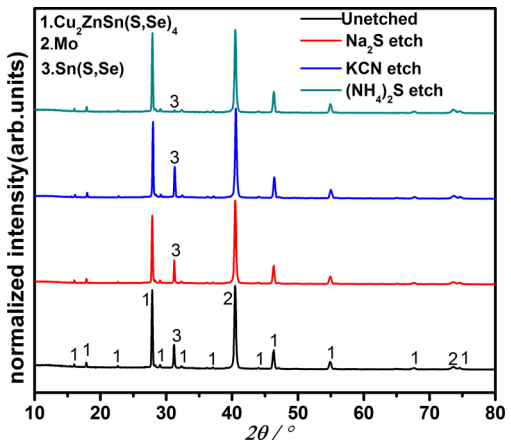

Figure 3. XRD of CZTSSe absorbers before and after etching. The concentrations of the solutions are 2% (w/v) KCN, 1 M Na_2S, and 22% (w/w) $(NH_4)_2S$. We use different units to express the concentrations in order to facilitate the preparation of each of them. In particular, the molarity of KCN and $(NH_4)_2S$ is not presented because the exact density of these solutions is unknown.

To demonstrate the selectivity of this process, the etching rate of different Sn binaries as well as CZTSSe is present in Table 2. The etching rate was determined using films prepared on glass (see the SI, part 2, for a detailed description of the methodology employed for the etch rate estimation) and measuring the thickness of these layers after different etching times by XRF. From Table 2, it is clear that the etching is very effective for the removal of SnS and SnSe [under the analyzed conditions: 22% (w/w) solution and room temperature], whereas it seems to be less effective for the SnS_2 and $SnSe_2$ phases. However, increasing the concentration of a $(NH_4)_2S$ solution or reaction temperature should be helpful for the improvement of the etching rate on SnS_2 and $SnSe_2$.[32] The kesterite phase is apparently not or very slightly etched, confirming the selectivity of the chemical process. It is important to remark that solubility tests were performed with powders of different secondary phases (ZnS, ZnSe, Cu_2Se, Cu_2S, SnSe, and SnS) and show that the solubility of the Zn and Cu binary compounds is negligible in this solution (see part 2.1 of the SI for a detailed description of the experiment).

Table 2. Etching Rate of 22% (w/w) $(NH_4)_2S$ on Sn−S, Sn−Se, and CZTSSe Thin Films

thin film	etching rate (nm/s)	thin film	etching rate (nm/s)
CZTSSe	<0.13	SnS	1.1
SnSe[a]	1.2	SnS_2[a]	0.5
$SnSe_2$	0.2		

[a]SnSe mixes with a little $SnSe_2$, and SnS_2 mixes with a little SnS. However, the conclusion is not affected. See the SI, part 2.

However, the process presented here also has effects on the morphology of the films (see Figure 4). Type 2 Sn binary phases are easily removed from the surface and do not have any apparent impact on the surface morphology. This is expected, taking into account that this type of secondary phase is a surface overgrowth. Nevertheless, the situation is different for the type 1 Sn binary secondary phases. After etching, there are some long trenches along the surface (see Figure 4b,c), which is the outline of the Sn(S,Se) rods after removal by yellow $(NH_4)_2S$. Note that these elongated trenches are shallow, and after removal, it is expected to have an impact only on the surface. However, no trace of the Sn(S,Se) phase with round shape (type 2) can be found (those corresponding to Figure 4a). This demonstrates that these two kinds of phases originated from different sources. The phases with elongated shape are most probably formed during the synthesis process, explaining why they are encrusted on the surface, while the other one may come from the condensation of Sn(S,Se) during the cooling process, explaining why it is on the surface of the films. When the annealing furnace is cooled down under vacuum, there are less type 2 secondary phases on the surface, which also supports this conclusion.

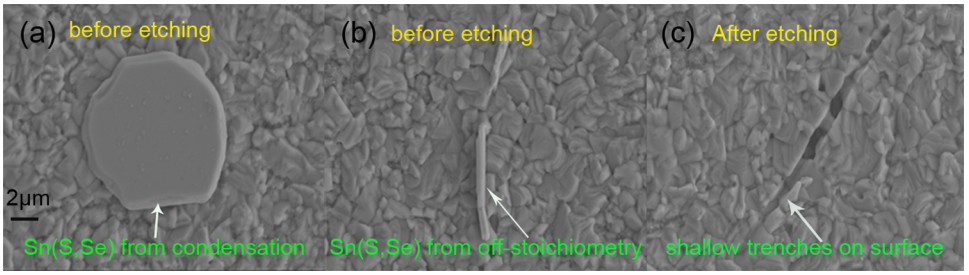

Figure 4. SEM images of type 2 (a) and type 1 (b) Sn(S,Se) secondary phases before etching on CZTSSe absorbers. (c) Surface image after removal of the type 1 Sn(S,Se) secondary phase with 22% $(NH_4)_2S$ chemical etching, showing the formation of shallow trenches.

The effectiveness of the etching process can be evaluated also with its impact on the global composition of the layers. Table 3

Table 3. Compositions of CZTSSe Absorbers before and after 22% (w/w) $(NH_4)_2S$ Etching by XRF

sample	Cu/(Zn + Sn)	Zn/Sn	thickness (μm)
unetched	0.86	1.22	1.73
$(NH_4)_2S$ etched	0.89	1.28	1.56

shows the composition of the absorbers before and after $(NH_4)_2S$ etching. After etching, both Cu/(Zn + Sn) and Zn/Sn increase, which is consistent with the removal of Sn(S,Se), i.e., with the diminution of the Sn concentration. The S/(S + Se) ratio seems to be unaffected by the etching, whereas the thickness slightly decreases, probably because of removal of the thin $SnSe_{0.8}S_{0.2}$ secondary phases on top of the layer. Similar changes in the thickness have been observed after etching of the ZnS and ZnSe phases on the surface and have been attributed to the removal of these phases.[17,19]

Note that the composition of the absorbers before etching measured by XRF differs from that obtained by EDS as mentioned before. This may be because XRF has a greater penetration depth than EDS, and Zn(S,Se) usually accumulates in the back, thus leading to lower Cu/(Zn + Sn) and higer Zn/Sn ratios in XRF measurements.[33]

To better understand the effect of etching in the CZTSSe-Sn(S,Se) system, it is important to analyze the route for the selective removal of Sn binaries. It was reported that yellow $(NH_4)_2S$ (namely, containing some S^0 traces) can dissolve SnS and SnS_2 via the formation of complexes.[34,35] Although not reported, considering the similar properties of S- and Se-based compounds, it is reasonable to suppose that SnSe [or Sn(S,Se)] behaves similarly. Tin(II) sulfide, selenide, or sulfoselenide will react with yellow ammonium sulfide, being oxidized to the tin(IV) state, forming the soluble ammonium thiostannate(IV) species (reaction I), and after with ammonia (reaction II), by means of the following reactions (the reactions are illustrated for the pure Se compounds but are analogues for the sulfide and sulfoselenide ones):

$$SnSe + S^{2-}{}_2S = SnSeS_2^{2-} \quad (I)$$

$$2NH_4^+ + SnSeS_2^{2-} = (NH_4)_2SnSeS_2(\text{soluble}) \quad (II)$$

Thus, using yellow $(NH_4)_2S$, the formation of soluble tin–ammonium chalcogenide complexes is the most probable chemical path for etching of the Sn binaries. Conversely, Cu and Zn complexes are not formed in the conditions studied in this work, probably because of the lower solubility of these compounds in an ammonia medium. It is important to remark that the use of colorless $(NH_4)_2S$ (without the presence of S^0) has a very limited impact on the solubility of tin chalcogenides and is considerably less effective for the removal of these secondary phases.

Improvements in the Optoelectronic Properties and Mechanism Discussion. To further investigate the role of Sn(S,Se) on the optoelectronic properties of CZTSSe solar cells, two different CZTSSe absorbers were prepared. CZTSSe1 has a little Sn(S,Se) content on the surface (check with SEM), while CZTSSe2 has a lot of Sn(S,Se) on the surface, as is described in the corresponding Experimental Section. With these two types of absorbers, devices were prepared with and without $(NH_4)_2S$ etching and $J-V$ curves were measured (see Figure 5a).

From Table 4, we can see that, after $(NH_4)_2S$ etching, the V_{oc}, J_{sc}, FF, and efficiency for CZTSSe1 devices increase

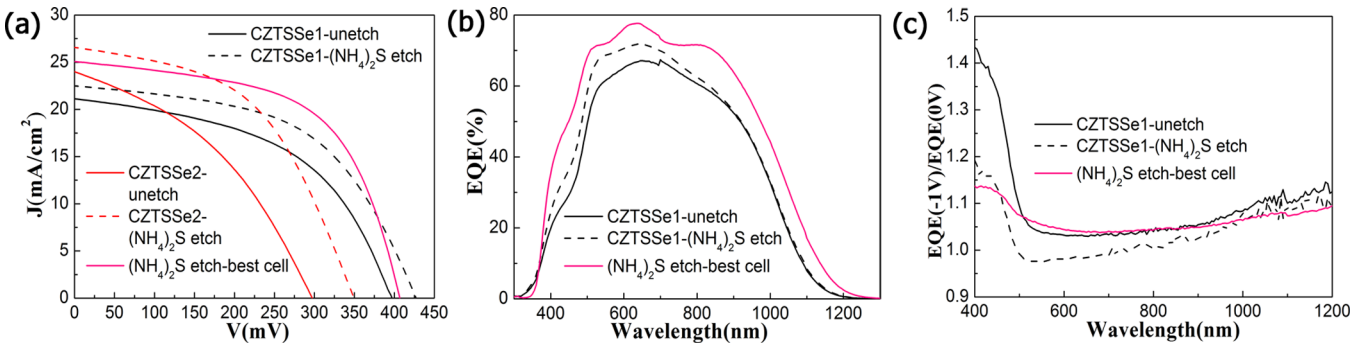

Figure 5. Illuminated $J-V$ curves of CZTSSe1 and CZTSSe2 solar cells before and after 22% (w/w) $(NH_4)_2S$ etching and the best solar cell obtained with the optimized process, producing a 5.9% efficiency device (a). EQE curves of CZTSSe1 and the best cell (b) and EQE(−1 V)/EQE(0 V) curves for CZTSSe1 and the best cell (c).

Table 4. Optoelectronic Properties of Devices before and after 22% (w/w) $(NH_4)_2S$ Etching

type	absorber	etching	J_{sc} (mA/cm^2)	V_{oc} (mV)	FF (%)	EFF (%)	R_s (Ω/cm^2)	R_{sh} (Ω/cm^2)	A	J_0 (mA/cm^2)
CZTSSe1	low Sn(S,Se) content on the surface	unetched	21.1	397	49.8	4.2	1.5	91	2.0	1.2×10^{-2}
		$(NH_4)_2S$ etched	22.4	427	52.9	5.1	2.6	142	1.7	2.1×10^{-3}
CZTSSe2	high Sn(S,Se) content on the surface	unetched	23.9	296	39.3	2.8				
		$(NH_4)_2S$ etched	26.5	349	49.5	4.6				
best cell		$(NH_4)_2S$ etched	25.1	406	57.6	5.9	0.7	109	1.7	1.4×10^{-3}

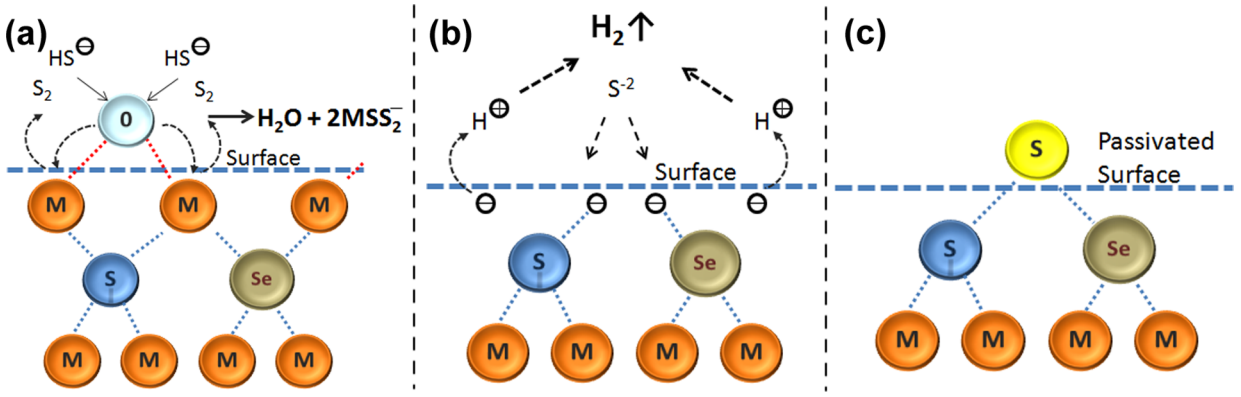

Figure 6. Schematic representation of passivation of the CZTSSe surface using yellow $(NH_4)_2S$ solutions: removal of the native oxides with the HS^- ions (a); electron transfer from the semiconductor toward the H^+ ions of the solution and production of H_2 (b); formation of the bond between the S and the dissolved chalcogen (c).

relatively by 7.6%, 6.2%, 6.2%, and 21.4%, respectively, while those for CZTSSe2 increase by 17.9%, 10.9%, 26%, and 64.2%, respectively. This shows that after etching all parameters were improved. Comparing the optoelectronic parameters of CZTSSe1 devices with those of CZTSSe2, we conclude that the higher the Sn(S,Se) quantity on the surface, the higher the V_{oc}, J_{sc}, and FF relative increase after etching. Nevertheless, the impact of the etching on J_{sc} is considerably less pronounced than that on V_{oc} and FF. This indicates that Sn(S,Se) mainly degrades V_{oc}, somehow also affecting FF of the devices because of, among others, the low band gap of this secondary phase. Additionally, R_s slightly changes, while R_{sh} markedly increases in the CZTSSe1 sample. Aside from the effect of Sn(S,Se) removal, the pronounced FF and R_{sh} increases could also be related to passivation effects of a $(NH_4)_2S$ solution on the surface of absorbers, as we will discuss below. After optimization of all processes, we obtain a cell with a maximum conversion efficiency of 5.9% (see the optoelectronic parameters in Table 4 and related curves in Figure 5), which is, to our knowledge, one of the highest values reported for a CZTSSe-based solar cell prepared from dc-sputtered metallic precursors. This efficiency, although still relatively low in comparison with the highest efficiencies reported in the literature for the CZTSSe solid solution based solar cells, is very encouraging, taking into account that the methodology presented here for the synthesis of CZTSSe absorbers is quite innovative. In ref 1, a 12.6% efficiency device was reported but using precursors containing S and a methodology involving the use of a highly toxic and explosive hydrazine compound. Additionally, other approaches using precursors containing S[2] and/or S−Se[8] compounds as precursors have reported efficiencies in the range of 6−9%. In our approach, we are using only metallic stacks as precursors, incorporating S and Se in a controlled manner using a one-step sulfoselenization process. In this sense, this methodology is suitable for the future industrial application of CZTSSe-based technologies and the obtained efficiencies are very encouraging for the future competitiveness of this technology. We have tested this etching with about 12 groups of devices, showing that the efficiency of all of the devices after etching increases by 20−65% relative to unetched values and depending on the quantity of Sn(S,Se) on the surface (the average increased value for the efficiency is 43% relative). In addition, the influence of the $(NH_4)_2S$ solution concentration on the optoelectronic properties of CZTSSe solar cells was also investigated, which shows that a 22% (w/w) $(NH_4)_2S$ solution is more effective than those with lower concentrations (see the SI, part 3.1).

To understand the improvements of the illuminated $J-V$ characteristics after $(NH_4)_2S$ etching, CZTSSe1 was analyzed to measure EQE with and without bias voltage. Parts b and c of Figure 5 show EQE and EQE(−1 V)/EQE(0 V) curves of CZTSSe1-based solar cells before and after $(NH_4)_2S$ etching. EQE shows that in the range 500−900 nm there are significant increases in EQE, which is consistent with the improvements of the p−n junction. From this EQE curve, we calculate the J_{sc} values, which are in very good agreement with those obtained from the $J-V$ illuminated curves (see the SI, part 3.2), indicating that there is a small influence of light-induced defects. Moreover, from Figure 5c, we know that after etching the EQE(−1 V)/EQE(0 V) curve is below that before etching, which means EQE is less dependent on the bias voltage, indicating that the device has better carrier collection efficiency. Note that EQE(−1 V)/EQE(0 V) curves increase considerably in the short-wavelength range for both samples, which is often associated with a low electron lifetime, or low field strength at the p−n interface, allowing electron back-diffusion into the p layer.[36] This problem is relatively well solved in the case of the best cell. In addition, ideality factor A and diode current density

J_0 were also extracted from the illuminated $J-V$ curves of the CZTSSe1 sample by Sites' method[37] and are shown in Table 4. After etching, A decreased from 2.0 to 1.7 and J_0 reduced almost one order of magnitude, which demonstrates better junction quality and less interface recombination in the device.

These results demonstrate that etching based in yellow $(NH_4)_2S$ has two beneficial effects on kesterites: (i) the selective removal of Sn binary secondary phases on the surface and (ii) the possible passivation of the surface. This passivation effect promoted by sulfide compounds has already been observed in III–V semiconductors[38−40] and very recently reported for CZTSe solar cells treated with Na_2S.[19] We propose a route for this passivation in the case of kesterites and using $(NH_4)_2S$ as a passivating agent, which implies the elimination of surface oxides and the formation of S passivated species. The mechanism is based on a three-step process, as shown in Figure 6. In the first step, the S ions (preferentially HS^- due to the pH of the solution) react with the surface metallic oxides, breaking the bond between the chalcogen and the metals as presented in Figure 6a, forming soluble metal chalcogenide species, and leaving H^+ ions in the solution. This process produces free bonds at the surface for subsequent bond formation with S ions from the $(NH_4)_2S$ solution. After dissolution of the native oxides, in a second step, the electrons from the conduction band of the semiconductor are transferred to the solution to neutralize the H^+ ions created in the previous step (Figure 6b), with the concomitant formation of $H_2(g)$, the formation of which is already observed during the etching process (formation of bubbles in the solution). This electron transfer allows the formation of chemical bonds between the S^{2-} free in the solution and the chalcogen atoms of the semiconductor (Figure 6c), explaining passivation of the surface. This mechanism explains the passivation effect of $(NH_4)_2S$ observed here and also reported previously for CZTSe with a Na_2S solution and is the key effect for the improvement of R_{sh} and FF presented in this work. A similar mechanism was proposed for III–V semiconductors.[41] However, it is the first time that we use the updated mechanism to explain the passivation effects of $(NH_4)_2S$ or Na_2S on chalcogenide-based solar cells. This opens a perspective for improvement of the CZTSSe/CdS heterojunction properties by elimination of the tail states in the kesterite surface before junction formation using yellow $(NH_4)_2S$ as a passivating agent.

CONCLUSIONS

In summary, in this paper we present a very effective chemical route using a yellow $(NH_4)_2S$ solution for the highly selective removal of Sn(S,Se) on the CZTSSe absorber surface. We find that Sn(S,Se) can form either from stoichiometric deviation or by condensation from the annealing atmosphere, which usually contains Sn and the chalcogens. We have shown that the presence of this detrimental secondary phase clearly degrades the performance of devices mainly because of the reduction of V_{oc}. Additionally, we report that the yellow $(NH_4)_2S$ solution not only is effective for the selective removal of Sn(S,Se) but also can passivate the surface, decrease interface recombination, and ultimately improve the p–n junction quality and the conversion efficiency of CZTSSe-based solar cells. We propose a surface passivation mechanism of CZTSSe with this type of solution, which can open new perspectives toward the preparation of high-efficiency devices with these kinds of earth-abundant absorbers.

ASSOCIATED CONTENT

Supporting Information

EDS measurements with 10 and 20 kV, powder solubility tests, XRD and etching curves of Sn–S, Sn–Se, and CZTSSe thin films, SEM and optoelectronic properties of CZTSSe etched with different concentrations of $(NH_4)_2S$, and comparison of J_{sc} from EQE and $J-V$ curves. This material is available free of charge via the Internet at http://pubs.acs.org.

AUTHOR INFORMATION

Corresponding Author

*E-mail: esaucedo@irec.cat.

Author Contributions

The manuscript was written through contributions of all authors. All authors have given approval to the final version of the manuscript.

Notes

The authors declare no competing financial interest.

ACKNOWLEDGMENTS

The research leading to these results has received funding from the People Program (Marie Curie Actions) of the European Union's Seventh Framework Program FP7/2007-2013/under REA Grant Agreement 316488 (KESTCELLS) and by European Regional Development Funds (ERDF; FEDER Programa Competitivitat de Catalunya 2007–2013). Authors from IREC and IN2UB belong to the M-2E (Electronic Materials for Energy) Consolidated Research Group and the XaRMAE Network of Excellence on Materials for Energy of the "Generalitat Generalitat de Catalunya". H.X. is thankful for a "China Scholarship Council" fellowship (CSC 201206340113), M.E.-R. for FPI-MINECO support (BES-2011-045774), D.S. for a PTA fellowship (PTA2011-5985-I), A.F. for a FPU fellowship (FPU12/05508), V.I.-R. for a "Juan de la Cierva" fellowship (JCI-2011-10782), and E.S. for a "Ramon y Cajal" fellowship (RYC-2011-09212).

REFERENCES

(1) Wang, W.; Winkler, M. T.; Gunawan, O.; Gokmen, T.; Todorov, T. K.; Zhu, Y.; Mitzi, D. B. Device Characteristics of CZTSSe Thin-Film Solar Cells with 12.6% Efficiency. *Adv. Energy Mater.* **2013**, *4*, 1301465.

(2) Wang, G.; Zhao, W.; Cui, Y.; Tian, Q.; Gao, S.; Huang, L.; Pan, D. Fabrication of a $Cu_2ZnSn(S,Se)_4$ Photovoltaic Device by a Low-Toxicity Ethanol Solution Process. *ACS Appl. Mater. Interfaces* **2013**, *5*, 10042–10047.

(3) He, J.; Lee, L.; Yang, S.; Li, Q.; Xiao, X.; Chen, T. Printable Highly Catalytic Pt- and TCO-Free Counter Electrode for Dye-Sensitized Solar Cells. *ACS Appl. Mater. Interfaces* **2014**, *6*, 2224–2229.

(4) Ma, G.; Minegishi, T.; Yokoyama, D.; Kubota, J.; Domen, K. Photoelectrochemical Hydrogen Production on Cu_2ZnSnS_4/Mo-mesh Thin-film Electrodes Prepared by Electroplating. *Chem. Phys. Lett.* **2011**, *501*, 619–622.

(5) Dudchak, I. V.; Piskach, L. V. Phase Equilibria in the CuSnSe–SnSe–ZnSe System. *J. Alloys Compd.* **2003**, *351*, 145–150.

(6) Olekseyuk, I. D.; Dudchak, I. V.; Piskach, L. V. Phase Equilibria in the Cu_2S–ZnS–SnS_2 System. *J. Alloys Compd.* **2004**, *368*, 135–143.

(7) Muska, K.; Kauk, M.; Altosaar, M.; Pilvet, M.; Grossberg, M.; Volobujeva, O. Synthesis of Cu_2ZnSnS_4 Monograin Powders with Different Compositions. *Energy Procedia* **2011**, *10*, 203–207.

(8) Chawla, V.; Clemens, B. Effect of Composition on High Efficiency CZTSSe Devices Fabricated Using Co-sputtering of Compound Targets. *IEEE Photovoltaic Spec. Conf.* **2012**, 002990–002992.

(9) Hsu, W.; Repins, I.; Beall, C.; DeHart, C.; Teeter, G.; To, B.; Yang, Y.; Noufi, R. The Effect of Zn Excess on Kesterite Solar Cells. *Sol. Energy Mater. Sol. Cells* **2013**, *113*, 160−164.
(10) Tanaka, T.; Sueishi, T.; Saito, K.; Guo, Q.; Nishio, M. Existence and Removal of Cu_2Se Second Phase in Coevaporated $Cu_2ZnSnSe_4$ Thin Films. *J. Appl. Phys.* **2012**, *111*, 053522.
(11) Fairbrother, A.; Fontané, X.; Izquierdo-Roca, V.; Espíndola-Rodríguez, M.; López, S.; Placidi, M.; Calvo-Barrio, L.; Pérez-Rodríguez, A.; Saucedo, E. On the Formation Mechanisms of Zn-rich Cu_2ZnSnS_4 Films Prepared by Sulfurization of Metallic Stacks. *Sol. Energy Mater. Sol. Cells* **2013**, *112*, 97−105.
(12) Lopez-Marino, S.; Placidi, M.; Perez-Tomas, A.; Llobet, J.; Izquierdo-Roca, V.; Fontane, X.; Fairbrother, A.; Espindola-Rodriguez, M.; Sylla, D.; Perez-Rodriguez, A.; Saucedo, E. Inhibiting the Absorber/Mo-back Contact Decomposition Reaction in $Cu_2ZnSnSe_4$ Solar Cells: the Role of a ZnO Intermediate Nanolayer. *J. Mater. Chem. A* **2013**, *1*, 8338−8343.
(13) Niki, S.; Fons, P. J.; Yamada, A.; Lacroix, Y.; Shibata, H.; Oyanagi, H.; Nishitani, M.; Negami, T.; Wada, T. Effects of the Surface $Cu_{2-x}Se$ Phase on the Growth and Properties of $CuInSe_2$ Films. *Appl. Phys. Lett.* **1999**, *74*, 1630.
(14) Schubert, B.; Marsen, B.; Cinque, S.; Unold, T.; Klenk, R.; Schorr, S.; Schock, H. W. Cu_2ZnSnS_4 Thin Film Solar Cells by Fast Coevaporation. *Prog. Photovoltaics* **2011**, *19*, 93−96.
(15) Weinhardt, L.; Fuchs, O.; Grob, D.; Umbach, E. Surface Modifications of $Cu(In,Ga)S_2$ Thin Film Solar Cell Absorbers by KCN and H_2O_2/H_2SO_4 Treatments. *J. Appl. Phys.* **2006**, *100*, 024907.
(16) Mousel, M.; Redinger, A.; Djemour, R.; Arasimowicz, M.; Valle, N.; Dale, P.; Siebentritt, S. HCl and Br_2-MeOH etching of $Cu_2ZnSnSe_4$ polycrystalline absorbers. *Thin Solid Films* **2013**, *535*, 83−87.
(17) Timmo, K.; Altosaar, M.; Raudoja, J.; Grossberg, M.; Danilson, M.; Volobujeva, O.; Mellikov, E. Chemical Etching of $Cu_2ZnSn(S,Se)_4$ Monograin Powder. *IEEE Photovoltaic Spec. Conf.* **2010**, 001982−001985.
(18) Fairbrother, A.; García-Hemme, E.; Izquierdo-Roca, V.; Fontané, X.; Pulgarín-Agudelo, F. A.; Vigil-Galán, O.; Peérez-Rodríguez, A.; Saucedo, E. Development of a Selective Chemical Etch to Improve the Conversion Efficiency of Zn-Rich Cu_2ZnSnS_4 Solar Cells. *J. Am. Chem. Soc.* **2012**, *134*, 8018−8021.
(19) López-Marino, S.; Sánchez, Y.; Placidi, M.; Fairbrother, A.; Espindola-Rodríguez, M.; Fontané, X.; Izquierdo-Roca, V.; López-García, J.; Calvo-Barrio, L.; Pérez-Rodríguez, A.; Saucedo, E. ZnSe Etching of Zn-Rich $Cu_2ZnSnSe_4$: An Oxidation Route for Improved Solar-Cell Efficiency. *Chem.—Eur. J.* **2013**, *19*, 14814−14822.
(20) Shin, S. W.; Pawar, S. M.; Park, C. Y.; Yun, J. H.; Moon, J.; Kim, J. H.; Lee, J. Y. Studies on Cu_2ZnSnS_4 (CZTS) Absorber Layer Using Different Stacking Orders in Precursor Thin Films. *Sol. Energy Mater. Sol. Cells* **2011**, *95*, 3202−3206.
(21) Xie, M.; Zhao, M.; Li, B.; Cao, M.; Song, J. Fabrication of Cu_2ZnSnS_4 Thin Films Using a Ceramic Quaternary Target. *Vacuum* **2014**, *101*, 146−150.
(22) Siebentritt, S. Why Are Kesterite Solar Cells Not 20% Efficient? *Thin Solid Films* **2013**, *535*, 1−4.
(23) Redinger, A.; Berg, D. M.; Dale, P. J.; Siebentritt, S. The Consequences of Kesterite Equilibria for Efficient Solar Cells. *J. Am. Chem. Soc.* **2011**, *133*, 3320−3323.
(24) Fairbrother, A.; Fontané, X.; Izquierdo-Roca, V.; Espindola-Rodriguez, M.; López- Marino, S.; Placidi, M.; López-García, J.; Pérez-Rodríguez, A.; Saucedo, E. Single-Step Sulfo-Selenization Method to Synthesize $Cu_2ZnSn(S_ySe_{1-y})_4$ Absorbers from Metallic Stack Precursors. *ChemPhysChem* **2013**, *14*, 1836−1843.
(25) Sharma, R. C.; Chang, Y. A. The S−Sn (Sulfur−Tin) System. *Bull. Alloy Phase Diagrams* **1986**, *7*, 269−273.
(26) Sharma, R. C.; Chang, Y. A. The Se−Sn (Selenium−Tin) System. *Bull. Alloy Phase Diagrams* **1986**, *7*, 68−72.
(27) Saucedo, E.; Izquierdo-Roca, V.; Ruiz, C. M.; Parissi, L.; Broussillou, C.; Grand, P. P.; Jaime-Ferrer, J. S.; Pérez-Rodríguez, A.; Morante, J. R.; Bermúdez, V. Key Role of Cu−Se Binary Phases in Electrodeposited $CuInSe_2$ Precursors on Final Distribution of Cu−S Phases in $CuIn(S,Se)_2$ Absorbers. *Thin Solid Films* **2009**, *517*, 2268−2271.
(28) Fontané, X.; Calvo-Barrio, L.; Izquierdo-Roca, V.; Saucedo, E.; Pérez-Rodriguez, A.; Morante, J. R.; Berg, D. M.; Dale, P. J.; Siebentritt, S. In-depth Resolved Raman scattering Analysis for the Identification of Secondary Phases: Characterization of Cu_2ZnSnS_4 Layers for Solar Cell Applications. *Appl. Phys. Lett.* **2011**, *98*, 181905.
(29) Redinger, A.; Hones, K.; Fontané, X.; Izquierdo-Roca, V.; Saucedo, E.; Valle, N.; Pérez- Rodríguez, A.; Siebentritt, S. Detection of a ZnSe Secondary Phase in Coevaporated $Cu_2ZnSnSe_4$ Thin Films. *Appl. Phys. Lett.* **2011**, *98*, 101907.
(30) Fairbrother, A.; Izquierdo, V.; Fontané, X.; Ibáñez, M.; Cabot, A.; Saucedo, E.; Pérez- Rodríguez, A. ZnS Grain Size Effects on Near-resonant Raman Scattering: Optical Non-Destructive Grain Size Estimation. *CrystEngComm* **2014**, *16*, 4120−4125.
(31) Fontané, X.; Izquierdo-Roca, V.; Fairbrother, A.; Espíndola-Rodríguez, M.; López-Marino, S.; Placidi, M.; Jawhari, T.; Saucedo, E.; Pérez-Rodríguez, A. Selective Detection of Secondary Phases in $Cu_2ZnSn(S,Se)_4$ Based Absorbers by Pre-resonant Raman Spectroscopy. *IEEE Photovoltaic Spec. Conf.* **2013**, 2581−2584.
(32) Seo, J.; Koker, T.; Agarwala, S.; Adesida, I. Etching Characteristics of $Al_xGa_{1-x}As$ in $(NH_4)_2S_x$ Solutions. *Appl. Phys. Lett.* **1992**, *60*, 1114−1116.
(33) Klenk, M.; Schenker, O.; Alberts, V.; Bucher, E. Control of Two-step Growth Processes of Chalcopyrite Thin Films by X-ray Fluorescence Spectroscopy. *Appl. Surf. Sci.* **2001**, *173*, 62−68.
(34) Raj, G. In *Advanced Inorganic Chemistry*, 31st ed.; Chatwal, M., Ed.; Krishna Prakashan Media: Meerut, Uttar Pradesh, India, 2008; Chapter 12, pp 506−601.
(35) Arora, A. *Text Book of Inorganic Chemistry*, 1st ed.; Discovery Publishing House: New Delhi, India, 2005; Chapter 14, pp 391−459.
(36) Hegedus, S. S.; Shafarman, W. N. Thin-Film Solar Cells: Device Measurements and Analysis. *Prog. Photovoltaics* **2004**, *12*, 155−176.
(37) Sites, J. R.; Mauk, P. H. Diode Quality Factor Determination for Thin-film Solar Cells. *Sol. Cells* **1989**, *27*, 411−417.
(38) Tseng, C.; Lee, C. Mechanisms of $(NH_4)_2S_x$-treated III−V Compound Triple-junction Solar Cells Incorporating with Hybrid Electrode. *Appl. Phys. Lett.* **2012**, *101*, 033902.
(39) Mariani, G.; Laghumavarapu, R. B.; Villers, B. T.; Shapiro, J.; Senanayake, P.; Lin, A.; Schwartz, B. J.; Huffaker, D. L. Hybrid Conjugated Polymer Solar Cells Using Patterned GaAs Nanopillars. *Appl. Phys. Lett.* **2010**, *97*, 013107.
(40) Lai, L.; Chen, J.; Lou, L.; Wu, C.; Lee, C. Performance Improvement of $(NH_4)_2S_x$-Treated III−V Compounds Multijunction Solar Cell Using Surface Treatment. *J. Electrochem. Soc.* **2008**, *155*, B1270−B1273.
(41) Bessolov, V. N.; Lebedev, M. Chalcogenide Passivation of III−V Semiconductor Surfaces. *Semiconductors* **1998**, *32*, 1141−1156.